

Alma Mater Studiorum Università di Bologna
Archivio istituzionale della ricerca

Description of the AC Loss Model for the ITER Central Solenoid During a Plasma Scenario

This is the final peer-reviewed author's accepted manuscript (postprint) of the following publication:

Published Version:

Bauer, P., Breschi, M., Cavallucci, L., Duchateau, J.L., Gauthier, F., Torre, A., et al. (2022). Description of the AC Loss Model for the ITER Central Solenoid During a Plasma Scenario. IEEE TRANSACTIONS ON APPLIED SUPERCONDUCTIVITY, 32(6), 1-5 [10.1109/TASC.2022.3157796].

Availability:

This version is available at: <https://hdl.handle.net/11585/907409> since: 2024-07-08

Published:

DOI: <http://doi.org/10.1109/TASC.2022.3157796>

Terms of use:

Some rights reserved. The terms and conditions for the reuse of this version of the manuscript are specified in the publishing policy. For all terms of use and more information see the publisher's website.

This item was downloaded from IRIS Università di Bologna (<https://cris.unibo.it/>).
When citing, please refer to the published version.

(Article begins on next page)

Development of an AC Loss Model for the ITER Central Solenoid during a Plasma Scenario

P. Bauer, M. Breschi, L. Cavallucci, J.L. Duchateau, F. Gauthier, A. Torre, B. Turck

Abstract -- AC loss is a major heat load in the pulsed, superconducting ITER coils, and thus a design driver for the cryo-system and superconductor. Given the importance of AC loss, extensive AC loss characterization of the components of the ITER coils, from the superconducting strands, cables, long “coil-like” conductors (so called insert-coils) to the completed coils, were conducted over the past years. Recently the first Central Solenoid (CS) modules were factory tested including AC loss tests representative of the operational conditions. The modelling of the AC loss is critical for the preparation of ITER Tokamak operation and commissioning. The following describes the AC loss models for the ITER CS coils. Such models need to be simple to implement and fast to execute to allow simulation of the long ITER plasma scenarios. The paper explains the simplifications applied and discusses the implications. Validations of the model on experimental data are presented.

Index Terms— Superconducting Magnets, AC loss, Nb₃Sn LTS, CICC, ITER.

I. INTRODUCTION

ITER is an international project located in the South of France which aims to demonstrate the feasibility of nuclear fusion for power generation. The ITER superconducting magnet system [1] is composed of 18 Nb₃Sn Toroidal Field (TF) coils, 6 NbTi Poloidal Field (PF) coils, 6 Nb₃Sn Central Solenoid (CS) Coils and 18 NbTi Correction Coils (CC). The TF coils generate the toroidal field needed for plasma confinement; the PF and CS coils generate the poloidal field required for plasma control and shaping; the CS also acts as the primary of a transformer inducing and maintaining the plasma current. The CC correct field errors due to positioning or manufacturing tolerances of the main coils. All these coils are cooled with supercritical Helium flowing at a temperature of ~4.5 K. The thermal loads in the magnet system have to be strictly controlled in order for the coils not to quench. These are mainly the static heat loads (radiation from the thermal shield and conduction through the supports), heating by stray neutrons from the fusion plasma and the AC loss, each representing about a third during a normal plasma scenario. Three AC loss contributions are being differentiated – the Joule heating due to eddy currents in the “passive” structures is not discussed further here (see [2] for a recent update). The two types of AC loss which occur in the superconducting cables, coupling and hysteresis losses, are the topic of discussion in this paper. The coupling losses are the result of induced currents flowing between filaments in the multi-filamentary

strands, and between strands within various cable stages as well as between sub-cables. Hysteresis (or “magnetization”) loss is caused by the diamagnetic shielding effect inside the superconductor in which persistent currents are induced to expel the applied magnetic field. The loss causing mechanism is the re-arrangement of screening currents and pinned magnetic field vortices due to a change of applied field. The coupling and hysteresis losses in the conductor average out to ~10 kW for the entire ITER coil system over the 1800 s reference plasma pulse (which includes ~500 s of fusion burn). This power, which needs to be compared to the 75 kW @ 4.2 K installed cryo-cooling capacity, is also comparable to the eddy current heat load in the passive structures. However, most of the coupling and hysteresis loss is deposited in the CS and PF coils, while the eddy current Joule heat is mostly deposited in the TF coil structures. During a normal plasma scenario, the AC loss in the CS coils is typically shared equally between plasma initiation/termination and the burn-phases. Note that a major plasma disruption produces approximately twice as much AC loss in the CS as for a full scenario, but within a few secs. It is therefore critical for the operational analysis of the ITER coils to assess the AC losses as input to thermo-hydraulic models to predict the minimum temperature margin in the superconductor for all these cases. In some cases it is only ~1 K, making the conductor vulnerable to excessive heat load (risk of quench).

In this paper we describe the coupling and hysteresis loss models developed over the years (see for example [3]-[6]) and which are now validated on as built CS modules. These models now need to be frozen for the preparation of the ITER commissioning and operations.

II. AC LOSS MODEL

Simulations of the AC loss through reconstruction of the complex induced current distributions from first principles, have been successfully attempted [7]-[9]. But this approach, a classical micro-macro scale problem with the CICC covering the range from tens of μm (sc filaments) to several tens or hundreds of m (cable length in coil), is not convenient for the (fast) simulation of plasma scenarios as for ITER which have order 100 k time points. The following therefore describes analytical approaches in which considerable simplification is achieved by using AC loss parameters measured in standardized tests on

conductor- (for coupling loss) or strand- (for hysteresis loss) samples. This phenomenological approach allows to bypass the calculation of the complex in-situ current distributions present in the conductor. Please also note that recent improvements on this type of model for coupling losses [10,11] are not considered at this time but it is understood that they may need to be considered for simulations of very fast events such as plasma disruptions. The AC loss power discussed in the following is per unit volume of superconducting strand (pure Cu strands are not counted). To obtain the total power, the power density needs to be multiplied by the number of superconducting strands, the strand cross-section and the length of conductor considered. Also to be noted is that the models for the two types of AC losses are somehow related, as the hysteresis loss model is needed to obtain the parameters of the coupling loss from the conductor sample tests, as they always appear together. This is described further in a companion paper discussing how the AC loss parameters for these models are obtained [12].

A. Coupling Loss

The loss causing coupling currents partially flow inside superconductor, which enhances their time constants and thus their strength considerably as compared to a normal conductor (on the other hand the normal conductor will have a much larger cross-section and thus loss for a given magnet performance). Therefore, in pulsed superconducting magnets as in ITER, all means possible to suppress these coupling currents are applied (twisting of the filaments, strands and sub-cables, applying resistive coatings of the strands, wrapping stainless steel foils over the sub-cables). But the coupling currents cannot be suppressed entirely, as this would lead to electrically insulated strands (or filaments), preventing the transfer of currents from saturated strands and thus lead to degraded performance and quench margin. According to [3, 4] the coupling loss power density per volume depends on the square of the local (“inner”) field variation dB_i/dt , and the L/R (inductance over resistance represented by the time constant τ) of the different coupling loops (see (1)). The temporal behavior of B_i , the “internal” locally applied field after taking into account the shielding by the eddy currents, is obtained from the externally applied field $B_e(t)$ from the solution of the simple ODE $B_i = B_e - \tau * dB_e/dt$. Here it is simply calculated iteratively from the previous B_i at time step $(t-\Delta t)$ by the finite differences method (but other more or less elaborate ways to calculate it exist). The externally applied field $B_e(t)$ along the conductor inside the coils is obtained from numerical analysis of the type as in [2]. The parameter describing the eddy current response of the cable is represented by $n\tau$, which is typically obtained from AC loss tests on conductor samples as discussed in [12] (or insert tests as discussed later). Equ. 2 gives the phenomenological fit used here.

$$p_{coupl} = \frac{n\tau}{\mu_0} \left(\frac{dB_i}{dt} \right)^2 \left[\frac{W}{m^3} \right] \quad \text{equ. (1)}$$

$$n\tau = n\tau_0 + \gamma \times B_e(T) + \lambda (B_e(T) \times I(kA)) [s] \quad \text{equ. (2)}$$

This fit takes into account that the loss time constant $n\tau$ increases at lower magnetic field, which is known to be related to

the magneto-resistance of the Cu in the strands. This dependence is assumed to be linear, with $n\tau_0$ the value at zero (applied) field and $\gamma(<0)$ the slope. The loss obviously also is larger in a cable under current compared to no current, as the Lorentz-force load compresses the cable favoring the contacts ($\lambda>0$). In the ITER Nb3Sn conductors, the coupling loss is highest in “virgin” condition. It strongly reduces as the bonds (sintered during the high temperature heat treatment of the coils to react the Nb3Sn from precursors) between the strands break during the first electromagnetic cycles. In ITER NbTi conductors for PF there is some evidence that the coupling loss increases with cyclic loading. This effect is not described by (2) (but further discussion can be found in [12]). Typically it is the $n\tau$ measured on conductor samples after cycling, which is implemented in scenario simulations (assuming that the coils will be brought into this state during the commissioning and pre-fusion plasma operation phases). In some particular cases the $n\tau$ for the virgin condition needs to be used (e.g. early stage of commissioning), such as in the experimental validation cases discussed below. The exact evolution of the loss in a specific ITER coil with the number of cycles between these two benchmark cases is generally not investigated given the large effort represented by each of these analyses.

B. Hysteresis Loss

The hysteresis loss depends on the so called “effective” filament diameter and the critical current density in the superconductor. The reduced filament sizes typical for LTS type strands (order 10 microns) cannot fully suppress this loss as the filaments are coupled through the Cu matrix (needed for electro-thermal stability of the strands) and thus behave like a larger filament. The critical current density should obviously be high enough to allow a large transport current to limit the superconductor cost. Since the superconductor is designed for the highest field region it can be over-designed for the low field regions in non-graded coil designs (as in ITER), additionally enhancing the hysteresis loss. The hysteresis loss calculation consists of integrating the magnetization M as a function of the applied field B_e . The instantaneous loss power is then as in (equ. 3, [11]), where ΔM is the width of the hysteresis loop from up- to down-field branch (the factor $1/2$ assumes the hysteresis loop is up/down symmetric). The magnetization is measured on single

$$p_{hyst} = \frac{1}{2} \Delta M(B_e, T, \epsilon) \frac{dB_e}{dt} \left[\frac{W}{m^3} \right] \quad \text{equ. (3)}$$

strand exposed to an applied field and the obtained magnetization loop is used to calculate the hysteresis loss of a cable where it is assumed that the applied field is the same for all strands in the cable. Alternatively, magnetization measurements could also be performed for entire cable samples, but this requires larger equipment (and therefore these measurements are less common). As also before for the coupling loss the magnetization is the response to the internal field B_i , which is not the same as the applied field B_e because of the shielding effect. For the single strand case it is relatively straightforward to estimate B_i from B_e as described in [12,13]. Two issues complicate the

computation of the hysteresis loss, however. The first is that the superconductor magnetization depends not only on field, but also on temperature T and, in Nb3Sn, on strain ε . Measurements of the magnetization for varying temperature and strain is experimentally complex. The work-around is provided by the above mentioned fact that M depends only on $J_c \times d_{eff}$, the product of the critical current density and the “effective” filament diameter. J_c is usually measured in strands as a function of T and ε (and B_e) in a transport measurement setting (recording the super-to-normal-conducting transition during a current ramp at fixed field). The transport type of measurement underestimates the J_c at low field, however, because the higher transport current a) produces a non-negligible magnetic self-field and b) combines with the shielding currents in a complex way making it difficult to relate B_i and B_e . Equ. 4 gives the J_c function finally used, which combines the field dependence obtained with $J_{c,mag}$ obtained from the magnetization test with the temperature and strain dependence from the $J_{c,transp}$, which is normalized to a reference temperature and strain to suppress the field dependence. Equ. 5 gives the instantaneous hysteresis loss power per volume of sc strand as a function of J_c . There the d_{eff} parameter is in fact a fitting parameter, which allows to bring into agreement the magnetization $J_{c,mag}$ (for low field) the transport $J_{c,transp}$ (for high field) and the magnetization M measurements. The J_c parameters in the model refer to the scaling laws as published in [13] for $J_{c,mag}$ and [14] for $J_{c,transp}$ (for Nb3Sn). Note that J_c is always referred to the non-Cu area in the superconducting strand. In Nb3Sn, in which the non-Cu area is further differentiated (diffusion barriers, non-reacted Sn) an additional parameter is introduced, k_{fil} , which is the non-Cu area divided by the Nb3Sn area,

$$J_{c,nonCu}(B_e, T, \varepsilon) = J_{c,nonCu,mag}(B_e) \times \frac{J_{c,nonCu,transp}(B_e, T, \varepsilon)}{J_{c,nonCu,transp}(B_e, T_0, -0.0022)} \left[\frac{A}{m^2} \right] \quad \text{equ. (4)}$$

$$p_{hyst,full} = \frac{2}{3\pi(1+CuNCu)} J_{c,nonCu}(B_e, T, \varepsilon) d_{eff} \frac{dB_e}{dt} \left[\frac{W}{m^3} \right] \quad \text{equ. (5)}$$

The second issue is that the magnetization response may not be fully developed, i.e. one is between the two branches of the magnetization loop (commonly referred to as the “partially penetrated” case). This condition is reached after a reversal of the sign of the dB_e/dt as long as ΔB_e has not allowed to reach the other side of the magnetization loop which by definition is $2B_p$ wide, with $B_p = \frac{\mu_0}{\pi} k_{fil} d_{eff} J_{c,nonCu}(B_e, T, \varepsilon)$ the so-called penetration field. During an ITER scenario the evolution of B_e can be very complex due to the plasma position feedback (incl. noise) and the complex electromagnetic interaction of the many (pulsed) coils and plasma. It is possible that the dB_e/dt changes sign a lot of times while in between the two branches. This kind of back and forth of the field produces very complex shielding current patterns with alternating signs inside the sc filaments (like onion layers) and a simplification is needed here also. Equ. 6 (a refinement of equ. 5) gives the instantaneous hysteresis loss per volume of sc strand in the partially penetrated case, as a

function of B_p . With the definition of B_p equ.6 can be brought into a form showing the dependence on $J_c \times d_{eff}$, see equ. 7.

$$p_{hyst,part} = \frac{B_p \frac{dB_e}{dt}}{2\mu_0 k_{fil} (1+CuNCu)} \left(\frac{\Delta B}{B_p} \right)^2 \left(1 - \frac{\Delta B}{3B_p} \right) \left[\frac{W}{m^3} \right] \quad \text{equ. (6)}$$

$$p_{hyst,part} = \frac{\pi \frac{dB_e}{dt} \Delta B^2}{2(1+CuNCu) \mu_0^2 k_{fil}^2 J_{c,nonCu}(B_e, T, \varepsilon) d_{eff}} \left(1 - \frac{\pi \Delta B}{3\mu_0 k_{fil} J_{c,nonCu}(B_e, T, \varepsilon) d_{eff}} \right) \left[\frac{W}{m^3} \right] \quad \text{equ. (7)}$$

Equ. 6&7 are rigorous, but the key parameter which will be simplified is ΔB , which is the change of applied field accumulated since the last sign reversal of dB_e/dt . Here the simplification applied is the following (also see the illustration in Fig. 1): as a dB_e/dt sign reversal occurs the magnetization loop branches are kept in memory for reference, denoted B_{sat+} and B_{sat-} , the first being the up-field branch and second the down branch. The difference $B_{sat+} - B_{sat-} = 2B_p$ per definition. As a simplification, the ΔB for a down-step in B_e is $\Delta B = B_{sat+} - B_e$ and for an up-step $\Delta B = B_e - B_{sat-}$. When $\Delta B_{\pm} \geq 2B_p$ the fully penetrated case is reached and $B_{sat\pm}$ are re-defined until the next sign reversal occurs. Note, that at this point B_p also changes with B_e through $J_c(B_e)$ - as B_e decreases, B_p increases. This change is distributed symmetrically (half/half) over the $B_{sat\pm}$ as can be seen between step 7&8 in Fig. 1. This approach to defining ΔB_{\pm} over-estimates ΔB , always referring it back to B_{sat} , while the step might

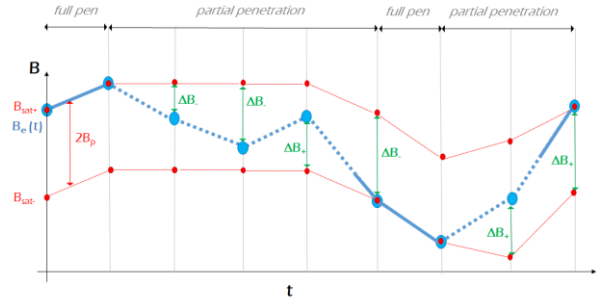


Fig. 1. Example of how ΔB is defined for the hysteresis loss calculation during a plasma scenario.

be much smaller. This simplification therefore results in a larger hysteresis loss and is conservative. The hysteresis loss generally does not change with number of cycles, but the presence of transport current reduces this loss (especially when closer to the critical current as in the high field regions). This so-called saturation effect is not modelled here.

C. Rotating Field

For the case of the ITER CS (and PF) coils the applied field can be decomposed into the two projections perpendicular to

the conductor, i.e. vertical and radial (there is no field component along the conductor). In first approximation the coupling loss can be calculated separately for the two components and added. In the case of the hysteresis loss this assumption does not hold, however, because the shielding current distribution in the superconducting filaments will always arrange in such a way as to cancel the applied field, i.e. it rotates with the field in the case of a rotating field. The sum of the field projections would generate a hysteresis loss that over-estimates the actual loss. A good example is the case of a purely rotating field. Assuming that the loss is driven by the applied field modulus would give zero loss, which is certainly too little. Assuming the radial field to decrease and the vertical to increase accordingly would mean integrating twice the magnetization, once for the decreasing field and once for the increasing, certainly too much. The so-called “rotating field” approach, which strictly speaking applies only to small rotations, projects the field onto a non-rotating ($B_{e,mod}$) and a rotating component ($B_{e,rot}$). Only the rotating component produces loss in the above case. The components of this applied field decomposition for which the separately computed hysteresis losses are added are given in equ. 8 and 9. The angle increment between each of the time steps $\delta\alpha$ is reported in equ. 10.

$$B_{e,mod}(t) = |\vec{B}_e| = \sqrt{B_{e,r}(t)^2 + B_{e,z}(t)^2} \quad [T] \quad \text{equ. (8)}$$

$$B_{e,rot}(t) = \sum dB_{e,rot}(t) = \sum \overline{B_{e,mod}(t)} \partial \alpha(t) \quad [T] \quad \text{equ. (9)}$$

$$\partial \alpha(t) = \arccos\left(\frac{\vec{B}_e(t) \cdot \vec{B}_e(t-\Delta t)}{B_e(t) B_e(t-\Delta t)}\right) \quad [rad] \quad \text{equ. (10)}$$

III. VALIDATION OF THE MODEL

The model described in II was validated through comparison with experiments. A general issue is that it is not possible to separate the coupling and hysteresis losses experimentally. But in fast ramps coupling losses dominate and in slow (or very short) ramps the hysteretic contribution dominates, as is clear from equ. 1&3. In the context of the so-called CS Insert (CSI) test campaign and the factory testing of the first two CS modules (CSM1&2) a number of fast discharges were performed which can readily be simulated with the model described above. Table I gives the general parameters of the CS coils and coupling loss parameters used in this case (CSI and CSM1 use the same conductor). Note that the AC loss parameters in Table I are for the coupling loss only as the coupling loss dominates for fast discharges. In the CSI the AC loss is induced in a ~40 m long sample (data shown are for the 4.5 m long central segment) by the discharge of the external coil (with zero current in the

TABLE I
AC LOSS PARAMETERS (FROM [12]) ITER CSI AND CSM1

Strand parameters from [15]	Number	Dia (mm)	Cu/NCu	NCu/Nb3Sn
	576	0.83/0.82	0.98/0.99	2.388/2.95
Loss param	n to (s)	n	γ (s/T)	λ (s/T-kA)
CSI, CSM1	0.590	2	-0.019	0.000113
CSM2	0.349	2	-0.015	0.000034

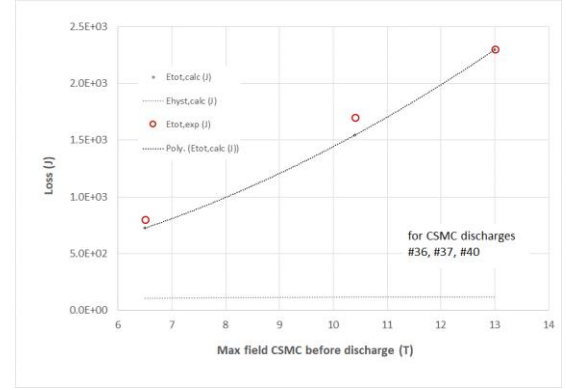


Fig. 2. CSI data and model comparison for discharges of the external field coil (loss energy for the 4.5 m central segment)

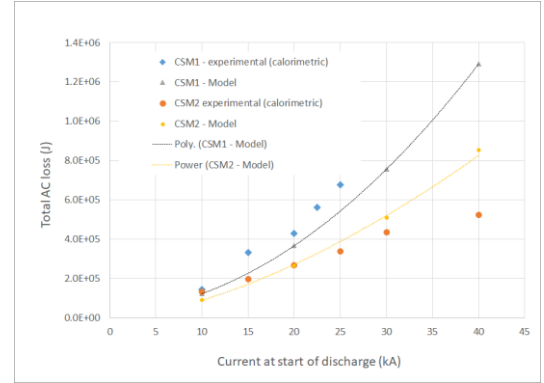


Fig. 3. CSM1 and CSM2 fast discharge data and model comparison (note the exp. discharge time constants are different for different currents).

insert in the cases considered in Fig. 2). In the CSM the condition is that of a fast discharge of the module, so it is the decaying transport current that generates the loss in the coil. With 554 turns the integrated loss is correspondingly larger than in the CSI (Fig. 3). Similar data to model comparisons are reported in [16],[17]. Note that the hysteresis loss is only of the order of ~10% in these cases, and there is no field rotation in both cases. This means that these data are only a weak validation of the hysteresis loss and rotating field models.

IV. SUMMARY AND OUTLOOK

Simple analytical AC loss models are needed for fast turn-around calculations for the large superconducting coils in the ITER device. Once validated on conductor and coil measurements such models can be used to simulate the AC loss heating during the plasma pulses. Such models were presented for the CS type ITER coils. In these coils the magnetic field transients are always transverse to the conductor, resulting in the simplest possible case. Models for field transients parallel to the conductor are needed to simulate the AC loss in other coils of the ITER system (TF, CC).

DISCLAIMER

The views and opinions expressed herein do not necessarily reflect those of the ITER Organization.

REFERENCES

- [1] N. Mitchell et al., "The ITER magnet system," *IEEE Transactions on Applied Superconductivity*, vol. 18, no. 2, pp. 435–440, 2008.
- [2] F. Cao et al., "Joule Losses in the ITER Cold Structures During Plasma Transients", *IEEE Transactions on Applied Superconductivity*, vol. 26, no. 4, 2016.
- [3] M. Wilson, "Superconducting magnet", Oxford Clarendon Press, 1983.
- [4] J. L. Duchateau, B. Turck, and D. Ciazynski, "Coupling-Current Losses in Composites and Cables: Analytical Calculations in Handbook of Applied Superconductivity, vol. 1, p. 212, B. Seeber, Ed. Bristol, U.K.: IOP Pub., 1998.
- [5] L. Bottura et al., "Computations of AC Loss in the ITER Magnets During Fast Field Transients", *IEEE Transactions on Applied Superconductivity*, Vol. 17, No. 2, 2007.
- [6] P. L. Bruzzone, "Superconductivity: Hysteresis and coupling losses," in *Engineering Superconductivity*, P. J. Lee, Ed. New York, NY, USA: Wiley Interscience pp. 138–152, 2001.
- [7] E. P. A. van Lanen, J. van Nugteren, and A. Nijhuis, "Full-scale calculation of the coupling losses in ITER size cable-in-conduit conductors," *Supercond. Sci. Technol.*, vol. 25, 2012, Art. no. 025012.
- [8] T. Bagni, A. Devred, A. Nijhuis, "Electromagnetic and thermal stability of the ITER Central Solenoid during a 15 MA plasma scenario", *Supercond. Sci. Technol.* 32, 085002, 2019.
- [9] M. Breschi et al., "Analysis of AC losses in the ITER central solenoid insert coil," *IEEE Trans. Appl. Supercond.*, vol. 27, no. 4, Jun. 2017, Art. no. 4200605.
- [10] L. Zani, B. Turck, "A macroscopic model for coupling current losses in cables made of multistages of superconducting strands and its experimental validation", *Cryogenics* 50 443–449, 2010
- [11] Louzguiti or Chilette paper also demonstrating the validity of B. Turcks formulae
- [12] A. Torre et al., "Review of experimental results and models for AC losses in the ITER PF and CS conductors", paper submitted to this conference
- [13] E. Seiler, "Hysteresis Losses and Effective $J_c(B)$ Scaling Law for ITER Nb3Sn Strands", *IEEE Trans. Appl. Supercond.*, vol. 26, no. 2, March 2016.
- [14] L. Bottura, B. Bordini, " $J_c(B,T,e)$ Parametrization for the ITER Nb3Sn Production", *IEEE TAS* Vol. 19, No. 3, 2009
- [15] Libeyre P et al., "Detailed design of the ITER Central Solenoid", *Fusion Eng. Des.* 84, 2009.
- [16] M. Breschi et al., "Analysis of AC Losses in the ITER Central Solenoid Insert Coil", *IEEE Transactions on Applied Superconductivity*, Vol. 27, No. 4, 2017
- [17] M. Breschi et al., "AC Losses in the First ITER CS Module Tests: Experimental Results and Comparison to Analytical Models, *IEEE Transactions on Applied Superconductivity*, Vol. 31, No. 5, 2021